

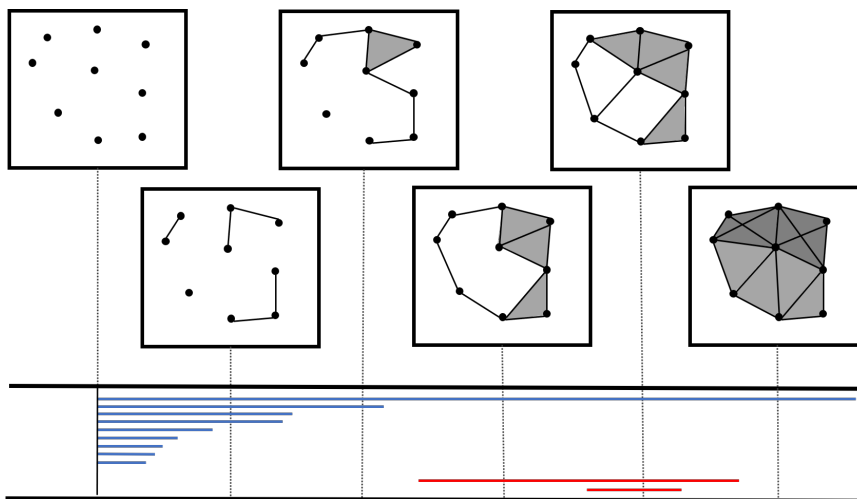
Persistence paths and signature features in topological data analysis

Ilya Chevyrev, Vidit Nanda, and Harald Oberhauser

ABSTRACT. We introduce a new feature map for barcodes that arise in persistent homology computation. The main idea is to first realize each barcode as a path in a convenient vector space, and to then compute its path signature which takes values in the tensor algebra of that vector space. The composition of these two operations — barcode to path, path to tensor series — results in a feature map that has several desirable properties for statistical learning, such as universality and characteristicness, and achieves state-of-the-art results on common classification benchmarks.

1. Introduction

Algebraic topology provides a promising framework for extracting nonlinear features from finite metric spaces via the theory of *persistent homology* [12, 21, 23]. Persistent homology has solved a host of data-driven problems in disparate fields of science and engineering — examples include signal processing [25], proteomics [11], cosmology [26], sensor networks [8], molecular chemistry [28] and computer vision [18]. The typical output of persistent homology computation is called a *barcode*, and it constitutes a finite topological invariant of the coarse geometry which governs the shape of a given point cloud.



For the purposes of this introduction, it suffices to think of a barcode as a (multi)set of intervals $[b_\bullet, d_\bullet)$, each identifying those values of a scale parameter $\epsilon \geq 0$ at which some topological feature — such as a connected component, a tunnel, or a cavity — is present when the input metric space is thickened by ϵ . A central advantage of persistent homology is its remarkable *stability* theorem [5, Ch. 5.6]. This result asserts that the map $\mathbf{Met} \rightarrow \mathbf{Bar}$ which assigns barcodes to finite metric spaces is 1-Lipschitz when its source and target are equipped with certain natural metrics.

Persistence paths and signature features. Notwithstanding their usefulness for certain tasks, barcodes are notoriously unsuitable for standard statistical inference because \mathbf{Bar} itself is a nonlinear metric space, and most scalable learning algorithms rely on linear methods. In this work, we construct a feature map of the form

$$\Phi_{\bullet} : \mathbf{Bar} \rightarrow \mathbf{T},$$

where $\mathbf{T} = \mathbf{T}(V)$ denotes the *tensor algebra* of a linear space V . The feature map Φ_{\bullet} is defined as composite, $\Phi_{\bullet} = S \circ \iota_{\bullet}$, of a *persistence path embedding* ι_{\bullet} and the *path signature* S ,

$$\mathbf{Bar} \xrightarrow{\iota_{\bullet}} \mathbf{BV}(V) \xrightarrow{S} \mathbf{T}(V),$$

where the intermediate space $\mathbf{BV}(V)$ contains all continuous maps $[0, 1] \rightarrow V$ of bounded variation.

Persistence path embedding ι_{\bullet} : The maps $\iota_{\bullet} : \mathbf{Bar} \rightarrow \mathbf{BV}(V)$ disambiguate our Φ_{\bullet} 's. There are many such embeddings, and they differ significantly in terms of stability, computability, and discriminative power.

Signature features S : The map S represents a path as its \mathbf{T} -valued *signature*. This map is injective (modulo natural equivalence classes of paths), provides a hierarchical description of a path, and has a rich algebraic structure that captures natural operations on paths, such as concatenation and time reversal.

The concept of a persistence path embedding ι_{\bullet} reflects the interpretation of persistent homology as a dynamic description of the topological features which appear and disappear as a metric space is thickened across various scales. There is precedent for such constructions; e.g. Bubenik's landscapes [3] can be reformulated to give an important example of such an ι_{\bullet} , which we denote with ι_{iL} . Despite their intuitive appeal, these approaches rely ultimately on a choice of feature map for paths, on which the resulting statistical learning guarantees depend.¹ We show here that the composition with the signature map resolves such issues. For example, one of our results is that the feature map $\Phi_{iL} = S \circ \iota_{iL}$ is

universal: non-linear functions of the data are approximated by linear functionals in feature space: for every (sufficiently regular) function $f : \mathbf{Bar} \rightarrow \mathbb{R}$ there exists ℓ in the dual of \mathbf{T} , such that $f(B) \approx \langle \ell, \Phi_{iL}(B) \rangle$ uniformly over barcodes B .

characteristic: the expected value of the feature map characterizes the law of the random variable: the map which sends a probability measure μ on \mathbf{Bar} to its expectation $\mu \mapsto \mathbb{E}_{B \sim \mu}[\Phi_{iL}(B)]$ in \mathbf{T} is injective.

stable: the map $\Phi_{iL} : \mathbf{Bar} \rightarrow \mathbf{T}$ has explicit continuity properties, as recorded in Theorems 2 and 5 below.

Perhaps the biggest advantage of our approach is that it is not limited to ι_{iL} . Besides ι_{iL} , we will also discuss the following path embeddings:

the naive embedding ι_N : sorts all intervals by length, enumerates them $\{1, \dots, n\}$, and forms an n -dimensional path by running in the i -th coordinate with unit speed if the i -th bar is active (otherwise remaining constant).

Euler embedding ι_{χ} : reduces a barcode to a single Euler characteristic curve (see [27, Sec. 3.2]). The resulting feature map Φ_{χ} is not stable, but is extremely fast to compute.

¹For example, [3] chooses a functional on the Banach space of paths, but how to choose such functionals in a non-parametric fashion and evaluate them efficiently remains unclear (unless something special is known a priori about the probability distribution of the observed barcodes).

Betti embedding ι_β : records only the Betti numbers as a function of the scale, and ignores information (contained in the barcode) which connects homology across different scale values.

envelope embedding ι_E : constructed by sorting the intervals $[b_\bullet, d_\bullet)$ of a barcode in descending order by length, and then assembling the ordered sequence of b_\bullet 's and d_\bullet 's into two separate paths. This appears to be a completely new embedding.

Analogous statements for universality and characteristicness hold for the other Φ_\bullet 's. Each of these embeddings ι_\bullet leads to different properties in terms of stability, computability, and discriminative power, for the associated feature maps Φ_\bullet . For example, Φ_E has neither the stability of Φ_{iL} nor the computability of Φ_χ , but it gives state-of-the-art performance on one of our supervised classification tasks. The emergence of a single feature map which is optimal along all three axes (stability, computability, discriminative power) appears unlikely, since these requirements tend to contravene each other. Stability requires the feature map to depend mostly on the longer intervals in a barcode, while in various problems (such as [11]), the signal of interest also resides in intervals of intermediate and short length.

Complexity, benchmarks and related work. The dimension of V varies significantly between the different persistence path embeddings. If a barcode contains $\approx 10^3$ intervals, ι_N would map it to a path in a $\approx 10^3$ -dimensional space, whereas ι_E always yields a path in 2 dimensions. Each of the above feature maps Φ_\bullet gives a *kernel* for barcodes $k_\bullet(B, B') := \langle \Phi_\bullet(B), \Phi_\bullet(B') \rangle$, and following [17], this kernel can be very efficiently computed regardless of $\dim(V)$ as long as V carries an inner product. However, for low-dimensional embeddings, Φ_\bullet can be computed directly and performs very well (e.g. giving state-of-the-art results on a standard orbit classification benchmark). We will describe the computational complexity in detail later, but we note here that all our experiments can be carried out on standard laptops.

Statistical learning from barcodes has received a lot of attention, see the background section in [1] for a recent survey. The most common theme is to construct a kernel for barcodes. We believe one strength our approach is the access to both, the kernel and its feature map (at least for the Betti, Euler, and envelope embeddings); the former gives access to well-developed tools from the kernel and Gaussian processes learning literature, while the latter allows us to use *any* learning method such as random forests or neural networks. A second advantage is that different choices of persistence path embeddings facilitates emphasis on different topological properties, and the feature space is a well-studied object (so in a supervised learning task, the optimal ι_\bullet can be determined by cross-validation).

Acknowledgements. IC is funded by a Junior Research Fellowship of St John's College, Oxford. VN's work is supported by The Alan Turing Institute under the EPSRC grant number EP/N510129/1, and by the Friends of the Institute for Advanced Study. HO is supported by the Oxford-Man Institute of Quantitative Finance. We are grateful to Steve Oudot and Mathieu Carrière for generously sharing their data [4] with us.

2. Background

As mentioned in the introduction, we construct maps of the form

$$\mathbf{Bar} \rightarrow \mathbf{BV}(V) \rightarrow \mathbf{T}(V),$$

from the space of persistence barcodes \mathbf{Bar} to the tensor algebra $\mathbf{T}(V)$ of V via the space of bounded variation paths \mathbf{BV} . In this section we define these three spaces and recall important properties; see [23, 5] resp. [19] for more details about \mathbf{Bar} resp. \mathbf{BV} .

2.1. Persistence, barcodes and stability. The *Vietoris-Rips* filtration [21, Sec. 3.1] associates a one-parameter nested family of finite simplicial complexes $\{K(t)\}_{t \geq 0}$ to each finite metric space (X, Δ) via the following rule. A subset $\{x_0, \dots, x_k\}$ of X spans a k -dimensional simplex in $K(t)$ if and only if all the pairwise distances satisfy $\Delta(x_i, x_j) < t$. Thus, one has the inclusion $K(t) \subseteq K(s)$ whenever $t \leq s$. Computing the homology of this family [15, Ch. 2] with coefficients in a field \mathbb{F} produces, in each dimension, a corresponding family of \mathbb{F} -vector spaces \mathbf{U}_\bullet as follows:

$$\mathbf{U}_\bullet(t) = H_\bullet(K(t); \mathbb{F}),$$

and inclusions of simplicial complexes induce linear maps $\mathbf{U}_\bullet(t) \rightarrow \mathbf{U}_\bullet(s)$ for $t \leq s$. This data consisting of vector spaces and linear maps indexed by real numbers is called a *persistence module*.

The following result from [29] uses the fact that the polynomial ring $\mathbb{F}[x]$ in one variable x acts on sufficiently tame persistence modules. Since this ring is a principal ideal domain, $\mathbb{F}[x]$ -modules have a particularly simple representation theory.

THEOREM 1 (Structure). *Under mild assumptions (always satisfied by Vietoris-Rips homology of finite metric spaces), each persistence module \mathbf{U} is completely characterized up to isomorphism by a finite collection of (not necessarily distinct) intervals $B = B(\mathbf{U}) = \{[b_\bullet, d_\bullet]\}$, called its barcode.*

Thus, a barcode is simply a multi-set containing some subintervals of $[0, \infty]$. When the persistence module in question comes from the Vietoris-Rips construction as described above, its barcode provides a complete summary of all the intermediate homology of $K(t)$ across $t \in [0, \infty)$. In particular, the i -th *Betti number* of $K(t)$, written

$$\beta_i^t = \dim H_i(K(t); \mathbb{F}), \tag{1}$$

equals the number of intervals in the i -dimensional barcode $B_i = \text{Bar}(\mathbf{U}_i)$ that contain t . Similarly, for $t \leq s$, the rank of the induced map on homology

$$\beta_i^{t,s} = \text{rank}(H_i(K(t); \mathbb{F}) \rightarrow H_i(K(s); \mathbb{F})) \tag{2}$$

equals the number of intervals in B_i that contain $[t, s]$.

There are several efficient algorithms which take as input finite metric spaces and produce as outputs the barcodes of their Vietoris-Rips filtrations [20, 13]. Concurrently, the theory has also developed at a rapid pace, and the following result [7, 5] is an exemplar of its progress. (Note that \mathbf{Met} is the collection of all finite metric spaces while \mathbf{Bar} is the collection of all barcodes containing finitely many intervals.)

THEOREM 2 (Stability). *The map $\text{PH}_i : \mathbf{Met} \rightarrow \mathbf{Bar}$ which assigns to each finite metric space its i -dimensional Vietoris-Rips persistent homology barcode is 1-Lipschitz for every $i \geq 0$. Here \mathbf{Met} is endowed with the Gromov-Hausdorff distance [14] while \mathbf{Bar} is endowed with the bottleneck distance (as defined in [7, Sec. 3.1]).*

Roughly, two barcodes lie within bottleneck distance ϵ of each other if it is possible to deform one to the other by moving the endpoints of all its intervals by at most ϵ (and vice-versa). Thus, the longer intervals are more stable to perturbation of the originating metric space (in particular, intervals of length smaller than 2ϵ might be created or destroyed during such a deformation).

2.2. Paths of bounded variation. Let V be a normed real vector space. Given a continuous path $x : [0, T] \rightarrow V$ (for some $T \geq 0$) and a finite partition of $[0, T]$

$$\bar{p} = (0 = p_0 \leq p_1 \leq \dots \leq p_{\ell-1} \leq p_\ell = T),$$

the 1-variation of x along \bar{p} is given by

$$\text{var}_1(x; \bar{p}) = \sum_{i=0}^{\ell-1} \|x(p_{i+1}) - x(p_i)\|_V.$$

DEFINITION 2.1. The total 1-variation of a continuous path $x : [0, T] \rightarrow V$ is defined as

$$\|x\|_{1\text{-var}} = \|x(0)\| + \sup_{\bar{p}} \{\text{var}_1(x; \bar{p})\},$$

where the supremum is taken over all finite partitions of $[0, T]$. The normed real vector space $\mathbf{BV}(V)$ consists of all continuous paths x that satisfy $\|x\|_{1\text{-var}} < \infty$, with addition and scalar multiplication being defined pointwise. The induced metric on $\mathbf{BV}(V)$ is given as usual by $\|x - y\|_{1\text{-var}}$.

Functions of bounded variation lie strictly between continuously differentiable and almost everywhere differentiable functions, and in particular every Lipschitz-continuous function $[0, T] \rightarrow V$ lies within $\mathbf{BV}(V)$.

2.3. The tensor algebra. Given a real vector space V and an integer $m \geq 0$, let $V^{\otimes m} = V \otimes V \otimes \cdots \otimes V$ denote the m -fold tensor product of V with itself. By convention, $V^{\otimes 0} = \mathbb{R}$. The tensor algebra $\mathbf{T}(V)$ of V is the direct product

$$\mathbf{T}(V) = \prod_{m \geq 0} V^{\otimes m}.$$

Thus, each element of $\mathbf{T}(V)$ is a sequence (v_0, v_1, \dots) where $v_m \in V^{\otimes m}$. We equip $\mathbf{T}(V)$ with the structure of a (graded) algebra under the tensor product operation, for which $V^{\otimes k} \otimes V^{\otimes \ell}$ takes values in $V^{\otimes(k+\ell)}$.

3. From barcodes to paths

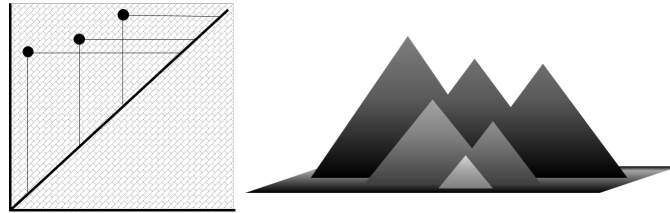
In this section we introduce several persistence path embeddings

$$\iota_\bullet : \mathbf{Bar} \rightarrow \mathbf{BV}(V).$$

To avoid technicalities, we make the following assumption (which is always met if B arises from the persistent homology of a finite metric space):²

ASSUMPTION 3.1. Assume that every barcode B encountered in this section is tame in two senses: first, it has only finitely many intervals, and second, each interval is contained within $[0, T_B]$ for some sufficiently large T_B .

3.1. The (integrated) landscape embedding. We first present an embedding with desirable stability properties. The persistence landscape of a barcode B is a single function $\Lambda : \mathbb{N} \times \mathbb{R} \rightarrow \mathbb{R}$, but it is often convenient to denote each $\Lambda(k, -) : \mathbb{R} \rightarrow \mathbb{R}$ by λ_k . The best introduction to landscapes is visual:



To the left is a barcode containing only three intervals, where each $[b, d)$ is shown as a point in the plane with coordinates (b, d) . The construction of three associated landscape

²The assumption can be sufficiently mollified, but since the underlying motivation for this work is computational and finitary, we do not lose any structure of interest by restricting to tame barcodes.

functions $\lambda_1 \geq \lambda_2 \geq \lambda_3 \geq 0$, which are shown to the right, proceeds by first projecting these points onto the diagonal, and then extracting successive maximal envelopes of the resulting arrangement of line segments. The higher λ_k for this illustrated barcode are all identically zero.

DEFINITION 3.2. [3, Def. 3] The **landscape** $\Lambda = \Lambda^B$ of the barcode B is the (continuous) function $\mathbb{N} \times \mathbb{R} \rightarrow \mathbb{R} \cup \{\infty\}$ given by

$$\Lambda^B(k, t) = \lambda_k^B(t) = \sup\{s \geq 0 \mid \beta^{t-s, t+s} \geq k\}.$$

Here, $\beta^{t-s, t+s}$ equals the number of intervals in B which contain $[t-s, t+s]$ (see (2) for the case of barcodes arising from persistent homology). Moreover, we adopt the usual convention that $\Lambda^B(k, t) = 0$ whenever the supremum is being taken over the empty set.

For tame barcodes B , one can safely exclude ∞ from the codomain of Λ^B . Moreover, each λ_k^B becomes bounded and compactly supported (in addition to continuous), so we may view the assignment of landscapes to barcodes as a function

$$\Lambda^\bullet : \mathbf{Bar} \rightarrow L^p(\mathbb{N} \times \mathbb{R})$$

for every $p \in [1, \infty]$. By [3, Thm. 12], Λ^\bullet is a 1-Lipschitz map when $p = \infty$ (using the bottleneck distance on its source and the sup-norm on its target). As a corollary, the stability theorem, recorded as Theorem 2 above for barcodes, extends further to landscapes.

DEFINITION 3.3. The **landscape embedding** $\iota_L : \mathbf{Bar} \rightarrow \mathbf{BV}(\ell^\infty)$ assigns to each landscape B a path $\iota_L(B)$ in $\mathbf{BV}(\ell^\infty)$ whose k -th component is the k -th landscape function for each $k \in \mathbb{N}$:

$$[\iota_L(B)]_k(t) = \lambda_k(t).$$

Similarly, the **integrated landscape embedding** $\iota_{iL} : \mathbf{Bar} \rightarrow \mathbf{BV}(\ell^\infty)$ is defined as

$$[\iota_{iL}(B)]_k(t) = \int_{-\infty}^t \lambda_k(s) ds.$$

The choice of $\mathbf{BV}(\ell^\infty)$ for the target space above is somewhat arbitrary: we may as well have mapped to $\mathbf{BV}(\ell^p)$ for any $p \in [1, \infty]$ or to $\mathbf{BV}(\mathbb{R}^n)$ via truncation. We now show that ι_{iL} inherits stability (in the sense of Theorem 2) from barcodes via their landscapes. The two spaces defined below will appear in the proof.

DEFINITION 3.4. For $p, q \in [1, \infty]$, define

- (1) the Banach space $L^{p,q}(\mathbb{N} \times \mathbb{R})$ consisting of all functions $y : \mathbb{N} \times \mathbb{R} \rightarrow \mathbb{R}$ for which the following (p, q) -norm is finite: $\|y\|_{L^{p,q}} = [\int_{\mathbb{R}} (\sum_{k=1}^{\infty} |y(k, t)|^p)^{q/p} dt]^{1/q}$, and
- (2) the Sobolev path space $W^{1,q}(\mathbb{R}, \ell^p)$ consisting of all functions $x : \mathbb{R} \rightarrow \ell^p$ for which there exists some $\dot{x} \in L^q(\mathbb{R}, \ell^p)$ such that $x(t) = \int_{-\infty}^t \dot{x}(s) ds$. The norm of x in this case is defined by $\|x\|_{W^{1,q}} = \|\dot{x}\|_{L^q}$.

At special values of p and q , the two spaces defined above become more familiar. For instance, $L^{p,p}(\mathbb{N} \times \mathbb{R})$ is the L^p space obtained by equipping $\mathbb{N} \times \mathbb{R}$ with the product of the counting and Lebesgue measures, as considered in [3, Sec. 2.4]. Similarly, $W^{1,\infty}(\mathbb{R}, \ell^p)$ is the space of 1-Hölder paths in ℓ^p , while $W^{1,1}(\mathbb{R}, \ell^p)$ is the subspace of absolutely continuous paths in $\mathbf{BV}(\ell^p)$. See [10, Sec. 1.4] for further details. In any case, landscapes in the image of Λ^\bullet lie in $L^{p,q}(\mathbb{N} \times \mathbb{R})$ for every possible $p, q \in [1, \infty]$.

LEMMA 3.5. For all $p, q \in [1, \infty]$, the map $\mathcal{J} : \Lambda(\star, \bullet) \mapsto \int_0^\bullet \Lambda(\star, s) ds$ is an isometry

$$L^{p,q}(\mathbb{N} \times \mathbb{R}) \xrightarrow{\cong} W^{1,q}(\mathbb{R}, \ell^p).$$

PROOF. The map $\varphi : L^{p,q}(\mathbb{N} \times \mathbb{R}) \rightarrow L^q(\mathbb{R}, \ell^p)$, $\varphi(y)(t) = (y(1,t), y(2,t), \dots)$, is an isometry:

$$\|y\|_{L^{p,q}}^q = \int_{\mathbb{R}} \left(\sum_{k=1}^{\infty} |y(k,t)|^p \right)^{q/p} dt = \int_{\mathbb{R}} \|\varphi(y)(t)\|_{\ell^p}^q dt = \|\varphi(y)\|_{L^q}^q.$$

By definition of $W^{1,q}(\mathbb{R}, \ell^p)$, the map $\int : L^q(\mathbb{R}, \ell^p) \rightarrow W^{1,q}(\mathbb{R}, \ell^p)$, $x \mapsto \int_{-\infty}^{\bullet} x(s) ds$, is also an isometry. The conclusion follows by observing that $\mathcal{J} = \int \circ \varphi$. \square

By recalling that all the Sobolev spaces $W^{1,q}(\mathbb{R}, \ell^p)$ lie in $\mathbf{BV}(\ell^p)$ (including $p = \infty$), the stability of ι_{IL} follows as a consequence.

THEOREM 3. The map $\mathbf{Met} \rightarrow \mathbf{BV}(\ell^\infty)$ obtained by composing the i -dimensional Vietoris-Rips persistent homology of Theorem 2 with the integrated landscape embedding of Definition 3.3, i.e.,

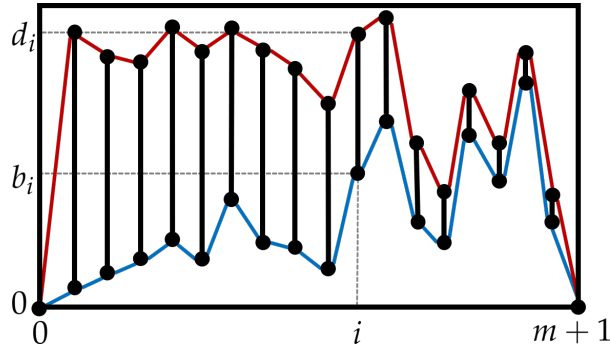
$$\mathbf{Met} \xrightarrow{\text{PH}_i} \mathbf{Bar} \xrightarrow{\Lambda^\bullet} L^\infty(\mathbb{N} \times \mathbb{R}) \xrightarrow{\iota_{\text{IL}}} \mathbf{BV}(\ell^\infty),$$

is 1-Lipschitz for every $i \geq 0$. Here \mathbf{Met} has the Gromov-Hausdorff metric while $\mathbf{BV}(\ell^\infty)$ has the 1-variation metric.

3.2. The envelope embedding. Consider $B \in \mathbf{Bar}$. Order the intervals $\{[b_i, d_i]\}_{i=1}^m$ of B in descending order by their lengths $(d_i - b_i)$, and embed them into \mathbb{R}^2 as the (disjoint) union

$$U(B) = \bigcup_{i=1}^m \{i\} \times [b_i, d_i].$$

The *upper envelope* $u_B : \mathbb{R} \rightarrow \mathbb{R}$ of B is the piecewise linear curve obtained by linearly interpolating between the highest points (i, d_i) of $U(B)$ across $i \in \{1, \dots, m\}$. Similarly, the *lower envelope* ℓ_B is obtained by interpolating between the lowest points (i, b_i) . We illustrate both envelopes in the accompanying figure, and remark that both curves are identically zero at t -values lying outside $[0, m+1]$.



DEFINITION 3.6. The **envelope embedding** is a map $\iota_E : \mathbf{Bar} \rightarrow \mathbf{BV}(\mathbb{R}^2)$ defined as follows. To each barcode B , it associates the path $\iota_E(B) : \mathbb{R} \rightarrow \mathbb{R}^2$, given by

$$[\iota_E(B)](t) = (\ell_B(t), u_B(t)).$$

Here u_B and ℓ_B are the upper and lower envelopes of B as described above.

For values of t near zero, the upper and lower envelopes, $\ell_B(t), u_B(t)$ capture only the longest, most stable intervals of B . As $t \geq 0$ increases, more of the smaller intervals get included, and the output $\iota_E(B)$ becomes more volatile to small perturbations of B (in the

bottleneck metric). This motivates us to truncate after a given time: pick an integer $N \geq 1$ and let $\iota_{\mathbb{E}}^N : \mathbf{Bar} \rightarrow \mathbf{BV}(\mathbb{R}^2)$ be the *restricted envelope embedding* obtained by setting

$$\iota_{\mathbb{E}}^N(B)(t) = \begin{cases} \iota_{\mathbb{E}}(B)(t) & \text{for } t \leq N, \\ (0, 0) & \text{for } t \geq N + 1, \text{ and} \\ ((N + 1 - t)u_B(N), (N + 1 - t)\ell_B(N)) & \text{for } N < t < N + 1. \end{cases}$$

If the feature map associated to this truncated envelope embedding performs well for small values of N and poorly for large ones, then one obtains evidence in favor of the hypothesis that the signal of interest genuinely resides in the larger, more stable intervals.

3.3. The Betti and Euler embeddings. In contrast to the previous two subsections, we now consider embeddings which depend on all homological dimensions.

DEFINITION 3.7. Denote $B = \bigcup_{i \geq 0} B_i$ where B_i contains all intervals of homological dimension i . Choose an integer $n \geq 1$ and numbers $a_i^k \in \mathbb{R}$ for $i \geq 0$ and $1 \leq k \leq n$. Setting $a = \{a_i^k\}$, the **generalised Betti embedding** $\beta(B; a) \in \mathbf{BV}(\mathbb{R}^n)$ is defined as follows. Let $\{t_j\}_{j=1}^m$ be the (ordered set of) all endpoints of intervals in B (which lie in $[0, T]$) together with $t_1 = 0$ and $t_m = T$. For each $j \in \{1, \dots, m\}$, set

$$\beta(B; a)(t_j) = \left(\sum_{i \geq 0} a_i^1 \beta_i^{t_j}, \dots, \sum_{i \geq 0} a_i^n \beta_i^{t_j} \right),$$

where $\beta_i^{t_j}$ is the Betti number of B as in (1). We extend the definition to points $t \in (t_j, t_{j+1})$ in a piecewise linear fashion

$$\beta(B; a)(t) = \beta(B; a)(t_j) + \frac{t - t_j}{t_{j+1} - t_j} \left(\beta(B; a)(t_{j+1}) - \beta(B; a)(t_j) \right).$$

The **Betti embedding** $\iota_{\beta}(B) \in \mathbf{BV}(\mathbb{R}^n)$ is defined by setting $a_i^k = 1$ if $k - 1 = i$ and $a_i^k = 0$ otherwise. The **Euler embedding** $\iota_{\chi}(B) \in \mathbf{BV}(\mathbb{R})$ is defined by setting $a_i^1 = (-1)^i$.

REMARK 3.8. When B arises from the persistent homology of a finite metric space, it is computationally convenient to recall that $\iota_{\chi} B(t_j)$ is the Euler characteristic of the associated Vietoris-Rips simplicial complex $K(t_j)$, and is thus also given by an alternating count of simplices across dimension:

$$\iota_{\chi}(B)(t_j) = \sum_{i \geq 0} (-1)^i \cdot \#\{i\text{-simplices in } K(t_j)\}.$$

Hence, $\iota_{\chi}(B)$ can be computed without knowing the actual homology of K . In fact, one could further consider generalised simplex embeddings

$$\sigma^k(B; a)(t_j) = \sum_{i \geq 0} a_i^k \cdot \#\{i\text{-simplices in } K(t_j)\},$$

which can all be computed without knowing the homology of K (albeit do not in general capture homological invariants).

REMARK 3.9. Since ι_{β} and particularly ι_{χ} are massive numerical reductions of B , it is apparent that metric spaces with very different persistence barcodes might have identical Betti and Euler embeddings. On the other hand, for barcodes arising from certain popular models of random metric spaces, the expected value of $|\iota_{\chi}(B)(t)|$ is a remarkably good predictor of the Betti number β_i^t for each $t \geq 0$ — see [16, Sec. 5.3] and the references therein for details.

4. From paths to tensors

We introduce the second component S for our feature map $\Phi_\bullet = S \circ \iota_\bullet$.

DEFINITION 4.1. For a Banach space V , the signature map is defined as

$$S : \mathbf{BV}(V) \rightarrow \mathbf{T}(V) \quad x \mapsto (S_0(x), S_1(x), \dots)$$

where $S_0(x) = 1$ and

$$S_m(x) := \int_{0 < t_1 < \dots < t_m < T} dx(t_1) \otimes dx(t_2) \otimes \dots \otimes dx(t_m) \in V^{\otimes m}$$

is defined as a Riemann–Stieltjes integral over the $m - 1$ simplex of length T .

EXAMPLE 4.2 (The case $V = \mathbb{R}^n$). For a path $x \in \mathbf{BV}(\mathbb{R}^n)$, it holds that

$$S_m(x) = \sum_{i_1, \dots, i_m} S^{i_1, \dots, i_m}(x) e_{i_1} \otimes \dots \otimes e_{i_m} \in (\mathbb{R}^n)^{\otimes m},$$

where the sum is taken over all multi-indexes $(i_1, \dots, i_m) \in \{1, \dots, n\}^m$, $(e_i)_{i=1}^n$ is a basis of \mathbb{R}^n , and

$$S^{i_1, \dots, i_m}(x) = \int_{0 < t_1 < \dots < t_m < T} dx_{i_1}(t_1) dx_{i_2}(t_2) \dots dx_{i_m}(t_m).$$

Hence the term $S_m(x)$ can simply be interpreted as a collection of n^m real numbers.

The mapping S is essentially injective up to a natural equivalence class of paths, called tree-like equivalence.³

THEOREM 4. [2] Let $x, y \in \mathbf{BV}(V)$. Then $S(x) = S(y)$ iff x and y are tree-like equivalent.

Tree-like equivalence can be a useful equivalence relation, e.g. it identifies paths that differ only by time-parametrization.⁴ For our applications, it is instructive to think of $S_m(x)$ as the natural generalisation of the monomial of order m of a vector $v \in V$ to pathspace.

EXAMPLE 4.3. Let $v \in \mathbb{R}^n$ and consider the path $x(t) = tv$ where $t \in [0, 1]$. The components of its signature are given by

$$S_m(x) = \int d(vt_1) \otimes \dots \otimes d(vt_m) = \int v^{\otimes m} dt_1 \dots dt_m = \left(\frac{v^{\otimes m}}{m!} \right),$$

Thus $S(x)$ indeed recovers the moment map $v \mapsto (1, v, \frac{v^{\otimes 2}}{2!}, \dots)$.

In analogy to monomials of vectors, one can ask whether linear combinations of such “monomials” $S_m(x)$ are dense in a space of functions, and, whether the sequence of expected “moments” characterizes the law of the random path. For compact subsets of $\mathbf{BV}(V)$, the answer to both question is yes, and follows by a standard Stone–Weierstrass argument; the general, non-compact case is more subtle (cf. classical moment problem) but is known to be true under suitable conditions [6].

³ x, y are tree-like equivalent iff there exists some \mathbb{R} -tree (i.e., a metric space in which any two points are connected by a unique arc which is isometric to a real interval) \mathfrak{T} so that $x * \overleftarrow{y}$, the concatenation of x with the time-reversal of y , decomposes as

$$[0, T] \xrightarrow{\phi} \mathfrak{T} \xrightarrow{\psi} V$$

where ϕ and ψ are continuous maps with $\phi(0) = \phi(T)$. We call a set of continuous paths in $\mathbf{BV}(V)$ *reduced* if none of its distinct elements are tree-like equivalent.

⁴ x and $x' = (x(\varphi(t)))$ are tree-like equivalent for any time-change φ .

5. Statistical learning

In this section we discuss the problem of statistical learning on the space of barcodes \mathbf{Bar} . The space \mathbf{Met} has traditionally been of more interest; however, since the persistent homology map $\text{PH} : \mathbf{Met} \rightarrow \mathbf{Bar}$ from Section 2.1 is well-understood, we focus here on \mathbf{Bar} . Results for \mathbf{Bar} -valued random variables pull back along PH to results for \mathbf{Met} -valued random variables.

We are interested in two standard learning problems: given independent random samples $B_1, \dots, B_k \sim B$ of a \mathbf{Bar} -valued random variable B , our aim is to

- (i) learn a function $f(B)$ of the data $f : \mathbf{Bar} \rightarrow \mathbb{R}$, and
- (ii) characterize the law μ of the data $B \sim \mu$.

As mentioned in the introduction, the standard approach to both problems is to find a feature map $\Phi : \mathbf{Bar} \rightarrow \mathbf{T}$ which is universal and characteristic (addressing points (i) and (ii) respectively). Let us establish these properties for our feature map

$$\Phi = S \circ \iota : \mathbf{Bar} \rightarrow \mathbf{T}(V),$$

where V is a Banach space, ι is any persistence path embedding (e.g., one of the maps from Section 3) and S is the signature map of Section 4. Due to the injectivity of S (up to tree-like equivalence), Φ preserves essentially all the information captured by ι . In particular, if ι maps some domain $\mathcal{D} \subset \mathbf{Bar}$ injectively into the space of tree-reduced paths (as is the case for any embedding once time is added as a coordinate), then Φ is also injective on \mathcal{D} . To make this precise, we use suitable quotient spaces.

DEFINITION 5.1. For $\iota : \mathbf{Bar} \rightarrow \mathbf{BV}(V)$, define the equivalence relation $B \sim_\iota B'$ iff $\iota(B)$ and $\iota(B')$ are tree-like equivalent. Let \mathbf{Bar}/ι denote the quotient of \mathbf{Bar} under this relation, and equip it with the initial topology (recall that $\mathbf{BV}(V)$ bears the 1-variation topology).

THEOREM 5. *Define*

$$\Phi : \mathbf{Bar}/\iota \rightarrow \mathbf{T}(V), \quad B \mapsto S \circ \iota(B).$$

On each compact subset $K \subset \mathbf{Bar}/\iota$, the map Φ has the following properties.

- (i) **(Universal)** *Let $f : K \rightarrow \mathbb{R}$ be continuous. For each $\epsilon > 0$, there exists ℓ in $\bigoplus_{m \geq 0} (V')^{\otimes m}$ (the dual space of the tensor algebra) such that*

$$\sup_{B \in K} |f(B) - \langle \Phi(B), \ell \rangle| < \epsilon.$$

- (ii) **(Characteristic)** *Denoting by \mathcal{M} the set of Borel probability measures on K , the map*

$$\mathcal{M} \rightarrow \mathbf{T}(V), \quad \mu \mapsto \mathbb{E}_{B \sim \mu} [\Phi(B)]$$

is injective.

- (iii) **(Kernelized)** *Suppose further that V is a Hilbert space. Then the map*

$$k : K \times K \rightarrow \mathbb{R}, \quad k(B, B') = \langle \Phi(B), \Phi(B') \rangle$$

defines a bounded, continuous kernel which is universal for the space of continuous functions $K \rightarrow \mathbb{R}$ and characteristic for Borel probability measures on K .

PROOF. The first two follow since the span of signature coordinates is closed under multiplication (in complete analogy to monomials spanning polynomials, the latter being dense among continuous function by Stone–Weierstrass) see [9, 6] for background. The kernelization was given in [17]. \square

The computational bottleneck for Φ is typically the calculation of the signature, since an element of $\mathbf{T}(V)$ truncated at level M needs $O(l \dim(V)^M)$ real numbers if $\iota(B)$ is assumed piecewise linear with at most l time points. This gets prohibitively large for

moderate dimensions. By contrast, the kernel on **Bar**, $k(B, B') = \langle \Phi(B), \Phi(B') \rangle$, is defined via the canonical inner product on $\mathbf{T}(V)$. Using [17], the level- M approximation to $k(B, B')$ can be computed in $O(l^2 c^2 M)$ time⁵ and $O(l^2)$ memory, where c is the cost of evaluating one inner product in V .

5.1. Hyperparameters. Each of the feature maps Φ_\bullet naturally generalises to a parametrised feature map Φ_\bullet^π where π denotes a set of parameters (which will be typically chosen by the learning algorithm). The set of parameters $\pi = \{M, \tau, \Delta, \phi\}$ are

- (1) $M \in \mathbb{N}$ is the *truncation level* of S , meaning that we only consider the first M components $(S_0(x), S_1(x), \dots, S_M(x))$ of every signature $S(x)$.
- (2) $\tau \in \{0, 1\}$ is the *time-augmentation* parameter. If it is non-zero, then we replace each path $x(t) \in \mathbf{BV}(V)$ by the path $(t, x(t)) \in \mathbf{BV}(\mathbb{R} \times V)$ before computing its signature.
- (3) $\Delta \in V^l$, for some $l \geq 0$, is a *lag vector* containing non-negative real numbers. We replace $x(t) \in \mathbf{BV}(V)$ by

$$(x(t), x(\max(t - \Delta_1, 0)), \dots, x(\max(t - \Delta_l, 0)))$$

in $\mathbf{BV}(V^{l+1})$ before computing its signature.

- (4) a *non-linearity* $\phi : V \rightarrow W$. Since ι_\bullet composed with a sufficiently regular map $\phi : V \rightarrow W$ to another vector space W , lifts barcodes to $\mathbf{BV}(W)$. If ϕ is injective and non-linear, one expects to obtain more efficient learning from signatures of paths in $\mathbf{BV}(W)$ since more non-linearities are provided by $S \circ \phi \circ \iota_\bullet(B) \in \mathbf{T}(W)$ than by $S \circ \iota_\bullet \in \mathbf{T}(V)$.⁶

For the choice $M = \infty$, $\tau = 0$, $\Delta = 0$ (with $l = 0$) and $\phi = \text{id} : V \rightarrow V$, the corresponding Φ^π recovers Φ , and $k^\pi(B, B') = \langle \Phi^\pi(B), \Phi^\pi(B') \rangle$ recovers k . With slight abuse of notation, we write Φ for Φ^π and k for k^π for the remainder of the article.

6. Experiments

We evaluate our feature map on two supervised classification tasks,⁷ orbits and textures, as described in Figures 1 and 2. For k_\bullet we throughout use support vector classifier (SVC), and for Φ_\bullet we use a random forest (RF).

6.1. Computational complexity. For a persistence path $\iota_\bullet(B) \in \mathbf{BV}(\mathbb{R}^n)$, truncation of the feature map $\Phi_\bullet(B)$ at tensors at level less or equal to M leads $O(n^M)$ coordinates (again, akin to classic polynomial features in machine learning). This combinatorial explosion limits the choice of $\iota \in \{\iota_E, \iota_\chi, \iota_\beta\}$ in practice: the integrated landscape embedding ι_{iL} produces paths in $\mathbf{BV}(\mathbb{R}^n)$ for large n , which rules out Φ_{iL} . However, the kernelization k_\bullet needs constant memory and computation time $O(Mn)$; in practice this allows us to evaluate up to $n \approx 10^2$ on standard laptops [17]; thus k_\bullet can be efficiently computed

⁵The low-rank approximation algorithm in [17] reduces this cost further to $O(lcM)$ time and $O(M)$ memory.

⁶Generically $\dim(W)$ will very high- or infinite-dimensional which prevents the direct calculation of $S \circ \phi \circ \iota_\bullet$. But if ϕ is the feature map of a kernel on V , (i.e. (W, κ) is a reproducing kernel Hilbert space over V with kernel $\kappa(u, v) := \langle \phi(u), \phi(v) \rangle$), then the signature kernelization [17] still allows to compute the kernel $k^\pi(B, B') = \langle \Phi^\pi(B), \Phi^\pi(B') \rangle$. Typically we choose $V = \mathbb{R}^n$ and use a classic kernel such as the RBF kernel.

⁷We hope to expand our experiments to other datasets for a more exhaustive benchmarking. One challenge, besides missing source code, is that it can be hard to replicate reported results in the literature: often preprocessing is done that is not further specified (e.g. on OUTEX various downsampling methods combined with CBLP preprocessing steps), the test-train split is unclear, etc. We used the same data set of barcodes and train-test split for all experiments.

for all ι_\bullet . On the other hand $\Phi_E(B)$, $\Phi_\chi(B)$, and $\Phi_\beta(B)$ are fast to compute directly since their ι 's produce low-dimensional paths.

6.2. Implementation. We implement our feature map Φ_\bullet and the kernel k_\bullet in Python's sci-kit learn package [24]. It takes as input a barcode B and the projection $\Phi_\bullet(B)|_M$ of $\Phi_\bullet(B)$ to $\prod_{m=0}^M(\mathbb{R}^n)^{\otimes m}$ (induced by truncating the signature map at the level $M \geq 1$) for any of the persistence path embeddings $\iota_\bullet \in \{\iota_E, \iota_\chi, \iota_\beta\}$.

For k_\bullet we use legacy code for [17, Alg. 3], but we did not implement the low-rank algorithm (which limits k_\bullet to paths with ≤ 300 time ticks on laptops, which is the reason why we don't report the kernel results for k_χ and k_β on the Orbits dataset); for $\Phi_\bullet|_M$ we make use of Terry Lyons' ESIG package. We also implemented the sliced Wasserstein kernel k_{SW} to reproduce the results reported in [4]. To avoid the quadratic growth of Gram matrix we used Nystrom for all kernels, our k_\bullet and the sliced Wasserstein k_{SW} . This allows for a reasonable benchmarking since [4] compares performance of k_{SW} against a large number of other methods and k_{SW} performs very well — see [4, Sec. 4.2 and 4.3].

6.3. Hyperparameter tuning. We use a grid search and 5-fold cross-validation for parameter tuning. The hyperparameter grid for Φ_\bullet^π consists of parameters π that are: the truncation level M in the tensor algebra, adding time; and if the kernelized version is used, then additionally the parameters of the kernel on V (we used throughout the Gauss kernel so this is just a $\sigma > 0$), together with the parameters of the classifier. Bigger grids are possible, e.g. including lags.

6.4. Performance. Tables 1 and 2 report the mean accuracy of repeating each experiment 20 times together with the standard deviation. As the results show, our features perform very competitively since k_{SW} provides a high benchmark⁸ (see [4] for a detailed comparison with other kernels).

Dataset	k_{SW}	k_E	k_χ	k_β
Textures	96.8 ± 1.0	$90.4 \pm 1.5(M=2)$	$94.9 \pm 0.6(M=3)$	$97.8 \pm 0.2(M=3)$
Orbits	94.6 ± 1.3	$96.6 \pm 0.9(M=2)$	NA	NA

TABLE 1. Mean accuracy (\pm standard deviation) using a SVC.

Dataset	$\Phi_E + \text{RF}$	$\Phi_\chi + \text{RF}$	$\Phi_\beta + \text{RF}$
Textures	$88.1 \pm 0.8(M=5)$	$92.9 \pm 0.7(M=8)$	$96.6 \pm 0.6(M=6)$
Orbits	$98.1 \pm 1.0(M=8)$	$98.8 \pm 0.6(M=7)$	$97.7 \pm 0.8(M=8)$

TABLE 2. Mean accuracy (\pm standard deviation) using random forests.

The best results for SW and E were achieved by looking at the 0th (vs 1st) homology. The values M in the parentheses represented the optimal truncation level in the tensor algebra (as chosen by cross-validated gridsearch); we ran all tests for $1 \leq M \leq 8$. The features Φ_\bullet performed best at higher levels, while k_\bullet performed best at lower levels. We suspect that the reason is that the Gaussian kernel non-linearity that lifts barcodes to paths in infinite-dimensional spaces, allows to capture the needed information already on level 2 or 3. We also ran the same experiments for the landscape and the naive embedding, ι_L and ι_N , but the results were not competitive on either dataset.

⁸Note that for k_{SW} , the results of our implementation achieve better accuracy, particularly for Orbits, than in the original paper [4], where it is 96.1 ± 0.4 for Textures and 83.7 ± 0.5 for Orbits. We believe this is due to a different Gram matrix approximation (we use Nystrom for all kernels) and longer running times. We wished to make a fair comparison with our methods, and therefore record the best possible performance for k_{SW} .

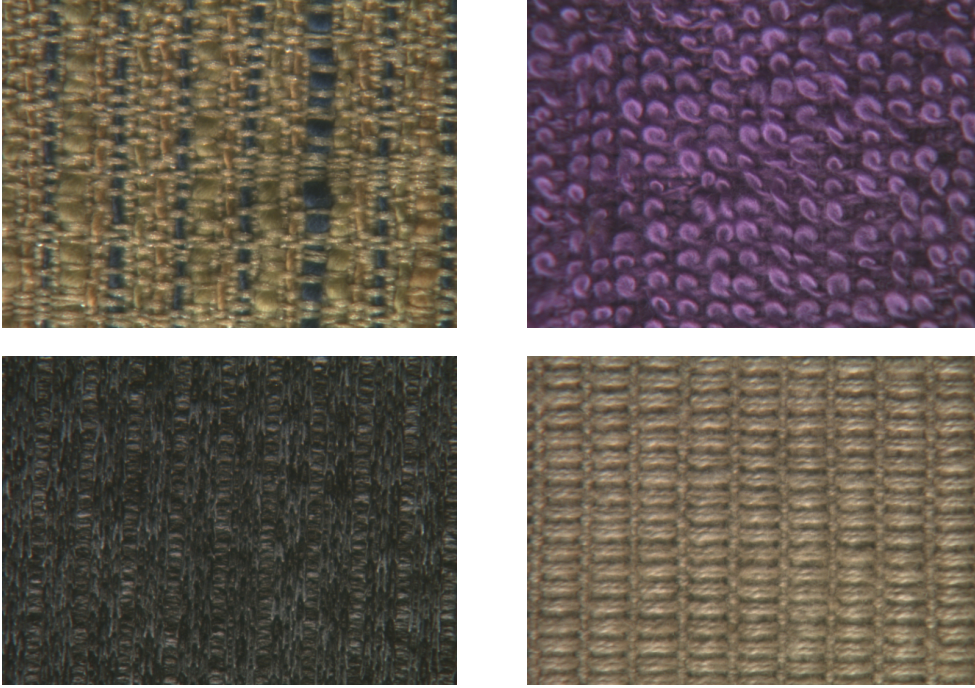


FIGURE 1. **Textures.** The *Outex_TC.00000* dataset of surface textures [22]. The data set consists of 240 images for training, 240 for testing, as prescribed by the test suite. Each sample carries one out of 24 labels. Above shows texture of four different labels.

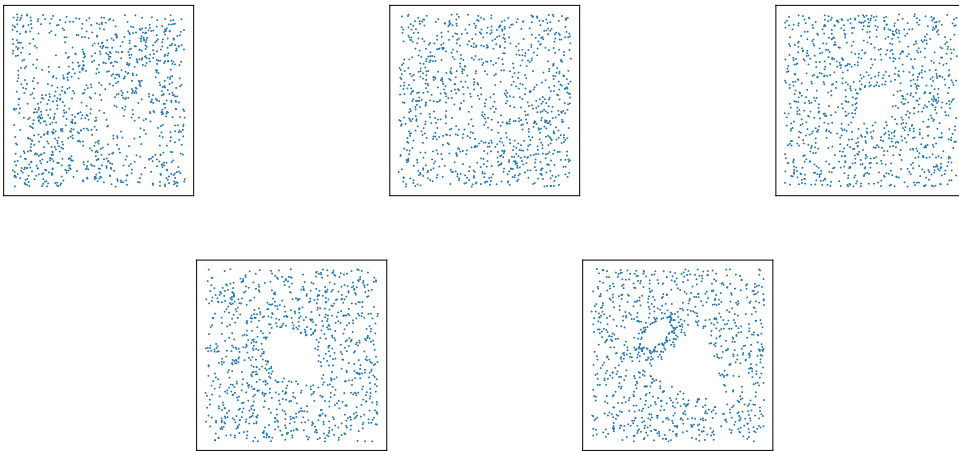


FIGURE 2. **Orbits.** The dataset consists of 500 orbits, $(x_n, y_n)_{n=0, \dots, 1000}$. Each orbit is generated by one out of five discrete dynamical systems with a random initial value (x_0, y_0) . The five dynamical systems are given by taking the parameter $r \in \{2.5, 3.5, 4, 4.1, 4.3\}$, which thus acts as label, and update rule $x_{n+1} = x_n + rx(1 - y_n) \bmod 1$, and $y_{n+1} = y_n + ry_n(1 - x_n) \bmod 1$ where (x_0, y_0) is chosen uniformly at random in $(0, 1)^2$. For each label r we generated 100 orbits and used 50% to 50% as train-test split for the resulting 500 orbits. Above shows one orbit for each $r = 2.5, 3.5, 4, 4.1, 4.3$ (left to right).

References

- [1] H. Adams, S. Chepushtanova, T. Emerson, E. Hanson, M. Kirby, F. Motta, R. Neville, C. Peterson, P. Shipman, and L. Ziegelmeier. Persistence Images: A Stable Vector Representation of Persistent Homology. *The Journal of Machine Learning Research*, 18(1):218–252, 2017.

- [2] H. Boedihardjo, X. Geng, T. Lyons, and D. Yang. The signature of a rough path: uniqueness. *Adv. Math.*, 293:720–737, 2016.
- [3] P. Bubenik. Statistical topological data analysis using persistence landscapes. *Journal of Machine Learning Research*, 16:77–102, 2015.
- [4] M. Carrière, M. Cuturi, and S. Oudot. Sliced Wasserstein kernel for persistence diagrams. In D. Precup and Y. W. Teh, editors, *Proceedings of the 34th International Conference on Machine Learning*, volume 70 of *Proceedings of Machine Learning Research*, pages 664–673, International Convention Centre, Sydney, Australia, 06–11 Aug 2017. PMLR.
- [5] F. Chazal, V. de Silva, M. Glisse, and S. Oudot. *Structure and stability of persistence modules*. Springer-Briefs in Mathematics. Springer, 2016.
- [6] I. Chevyrev and T. Lyons. Characteristic functions of measures on geometric rough paths. *Ann. Probab.*, 44(6):4049–4082, 2016.
- [7] D. Cohen-Steiner, H. Edelsbrunner, and J. Harer. Stability of persistence diagrams. *Discrete and Computational Geometry*, 37(1):103–120, 2007.
- [8] V. de Silva and R. Ghrist. Coverage in sensor networks via persistent homology. *Algebraic and Geometric Topology*, 7(1):339–358, 2007.
- [9] T. Fawcett. *Problems in stochastic analysis: connections between rough paths and non-commutative harmonic analysis*. PhD thesis, University of Oxford, 2003.
- [10] P. K. Friz and N. B. Victoir. *Multidimensional stochastic processes as rough paths: theory and applications*. Cambridge Studies in Advanced Mathematics. Cambridge University Press, Cambridge, 2010.
- [11] M. Gameiro, Y. Hiraoka, S. Izumi, M. Kramar, K. Mischaikow, and V. Nanda. A topological measurement of protein compressibility. *Japan Journal of Industrial and Applied Mathematics*, 32(1):1–17, 2015.
- [12] R. Ghrist. Barcodes: the persistent topology of data. *Bulletin of the American Mathematical Society*, 45(1):61–75, 2008.
- [13] R. Ghrist and G. Henselman. Matroid filtrations and computational persistent homology. *arXiv:1606.00199v2[math.at]*, 2016.
- [14] M. Gromov. Groups of polynomial growth and expanding maps. *Inst. Hautes Études Sci. Publ. Math.*, 53:53–73, 1981.
- [15] A. Hatcher. *Algebraic topology*. Cambridge University Press, 2002.
- [16] M. Kahle. Topology of random simplicial complexes: a survey. *AMS Contemporary Math*, 620:201–222, 2014.
- [17] F. J. Király and H. Oberhauser. Kernels for sequentially ordered data. *ArXiv e-prints*, 1601.08169, 2016.
- [18] J. Lamar-Leon, R. Alonso-Baryolo, E. Garcia-Reyes, and R. Gonzalez-Diaz. Persistent homology-based gait recognition robust to upper body variations. In *2016 23rd International Conference on Pattern Recognition (ICPR)*, pages 1083–1088, Dec 2016.
- [19] T. J. Lyons, M. Caruana, and T. Lévy. Differential equations driven by rough paths, 2007. Lectures from the 34th Summer School on Probability Theory held in Saint-Flour, July 6–24, 2004, With an introduction concerning the Summer School by Jean Picard.
- [20] K. Mischaikow and V. Nanda. Morse theory for filtrations and efficient computation of persistent homology. *Discrete and Computational Geometry*, 50(2):330–353, 2013.
- [21] V. Nanda and R. Sazdanović. Simplicial models and topological inference for biological systems. In N. Jonoska and M. Saito, editors, *Discrete and Topological Models in Molecular Biology*, chapter 6, pages 109–141. Springer, 2014.
- [22] T. Ojala, T. Maenpaa, M. Pietikainen, J. Viertola, J. Kyllonen, and S. Huovinen. Outex-new framework for empirical evaluation of texture analysis algorithms. In *Pattern Recognition, 2002. Proceedings. 16th International Conference on*, volume 1, pages 701–706. IEEE, 2002.
- [23] S. Oudot. *Persistence theory: from quiver representations to data analysis*, volume 209 of *Mathematical Surveys and Monographs*. American Mathematical Society, 2015.
- [24] F. Pedregosa, G. Varoquaux, A. Gramfort, V. Michel, B. Thirion, O. Grisel, M. Blondel, P. Prettenhofer, R. Weiss, V. Dubourg, J. Vanderplas, A. Passos, D. Cournapeau, M. Brucher, M. Perrot, and E. Duchesnay. Scikit-learn: Machine learning in Python. *Journal of Machine Learning Research*, 12:2825–2830, 2011.
- [25] J. A. Perea and J. Harer. Sliding windows and persistence: An application of topological methods to signal analysis. *Foundations of Computational Mathematics*, 15(3):799–838, Jun 2015.
- [26] T. Sousbie. The persistent cosmic web and its filamentary structure – I. Theory and implementation. *Monthly Notices of the Royal Astronomical Society*, 414(1):350–383, 2011.
- [27] K. Turner, S. Mukherjee, and D. M. Boyer. Persistent homology transform for modeling shapes and surfaces. *Information and Inference: A Journal of the IMA*, 3(4):310–344, 2014.

- [28] K. Xia, X. Feng, Y. Tong, and G. W. Wei. Persistent homology for the quantitative prediction of fullerene stability. *Journal of Computational Chemistry*, 36:408–422, 2015.
- [29] A. Zomorodian and G. Carlsson. Computing persistent homology. *Discrete and Computational Geometry*, 33:249–274, 2005.

MATHEMATICAL INSTITUTE, UNIVERSITY OF OXFORD
E-mail address: chevrev@maths.ox.ac.uk

MATHEMATICAL INSTITUTE, UNIVERSITY OF OXFORD, AND SCHOOL OF MATHEMATICS, INSTITUTE
FOR ADVANCED STUDY
E-mail address: nanda@maths.ox.ac.uk

MATHEMATICAL INSTITUTE, UNIVERSITY OF OXFORD
E-mail address: oberhauser@maths.ox.ac.uk